Robust Path-following Control with Anti-Windup for HALE Aircraft

Christian Weiser[1], Daniel Ossmann[2], and Harald Pfifer[3]

***Abstract*— In this paper, a robust path-tracking controller for a High Altitude Long Endurance (HALE) aircraft is presented. The main control paradigm for operating a HALE aircraft consists of a basic path following control, i.e. tracking a reference flight path and airspeed while dealing with very limited thrust. The priority lies in keeping airspeed inside the small flight envelope of HALE aircraft even during saturated thrust. For the basic path following objective, a mixed sensitivity approach is proposed which can easily deal with decoupled tracking and robustness requirements. To deal with saturated control inputs, an anti-windup scheme is incorporated in the control design. A novel observer-based mixed sensitivity design is used which allows directly using classical anti-windup methods based on back-calculation. The control design is verified in nonlinear simulation and compared to a classical total energy control based controller.**

I. Introduction

High Altitude Long Endurance (HALE) aircraft are usually operated on multi-day missions, where the goal is to track a specific reference flight path whilst flying at the airspeed for maximum aerodynamic efficiency. This is needed in order to minimize the necessary weight of solar generators and batteries. Due to the likewise minimized structural weight, the airspeed envelope is very small. This is extremely critical, as it requires accurate tracking of the airspeed reference throughout maneuvering and especially during disturbances, e.g. gusts or continuous turbulence.

The contribution of this paper is the proposal of an observer-based mixed sensitivity flight path-tracker. The observer-based design has the advantage, that including anti-windup becomes a fairly easy task. The design follows an approach presented in [1]. The resulting path-tracker is then connected to an inner cascade consisting of an attitude controller introduced in [2].

The first part of the paper introduces the observer-based mixed sensitivity control design [1]. Furthermore, anti-windup methods are discussed which are crucial for a successful implementation in the aircraft path-tracking application, as limitation especially in the thrust command variable is expected. In a second step, the dynamics of the example platform are introduced. The aircraft is currently being developed by the German Aerospace Center [3]. The path-tracker mixed-sensitivity synthesis presented in section II is applied to the longitudinal aircraft dynamics model which is already augmented by the previously described pitch attitude tracker. Furthermore, anti-windup compensation is added in order to obtain a control design which shows adequate performance especially in presence of thrust saturation. Finally, the obtained mixed-sensitivity path-tracker is verified in the non-linear domain and compared to results obtained with the previously implemented Total Energy Control System (TECS) algorithm designed in [2].

[1]Christian Weiser is with the Institute of System Dynamics & Control, German Aerospace Center (DLR), Weßling, Germany christian.weiser@dlr.de

[2]Daniel Ossmann is with the Department of Mechanical, Automotive & Aerospace Engineering, Munich University of Applied Sciences HM, Munich, Germany daniel.ossmann@hm.edu

[3]Harald Pfifer is with the Chair of Flight Mechanics & Control, TU Dresden, Dresden, Germany harald.pfifer@tu-dresden.de

II. Observer Based Mixed Sensitivity Control with Anti-Windup

A. Mixed sensitivity controller synthesis

Shaping closed loop sensitivity functions through minimization of the H_∞-norm is a common approach for control design in literature, see e.g. [4]. A common interconnection for designing the controller $K(s)$ is given in terms of a mixed sensitivity problem in Fig. 1. The considered plant $G(s)$ can be augmented by an explicit disturbance model $G_d(s)$, as depicted in the figure. The mixed sensitivity formulation is the weighted closed loop system's H_∞-norm of the feedback interconnection in Fig. 1 [4], which can be noted as follows:

$$\begin{bmatrix} z_e \\ z_u \end{bmatrix} = \begin{bmatrix} W_e V_e^{-1} & 0 \\ 0 & W_u V_u^{-1} \end{bmatrix} \begin{bmatrix} S & -SG_d \\ KS & -KSG_d \end{bmatrix} \begin{bmatrix} V_e & 0 \\ 0 & W_d \end{bmatrix} \begin{bmatrix} r \\ d \end{bmatrix}, \tag{1}$$

where $S = (I + GK)^{-1}$ denotes the output sensitivity function. The weighting scheme differentiates between frequency dependent weights denoted by W and constant scaling factors denoted by V. It is taken from [5]. The weight function W_e enforces the frequency requirements on the sensitivity function, i.e. tracking and disturbance rejection at low frequencies. The weight W_u shapes the control input u through KS. It can be used to enforce an appropriate roll-off of the controller K. The scalings V_e, V_u and V_d can be used for setting the maximum allowable control error, control effort and disturbance, respectively.

B. Observer-based mixed sensitivity synthesis

In general, solving the output feedback mixed sensitivity problem defined in the previous section results in a full order controller without specific structure. However, the output feedback problem can be separated in an observer and a state-feedback problem while retaining the closed loop shaping characteristics. The main result of this separation goes back to H_∞ loop-shaping by Glover and McFarlane [6] and [7]. More recently, observer-based mixed sensitivity control techniques have been proposed for linear parameter

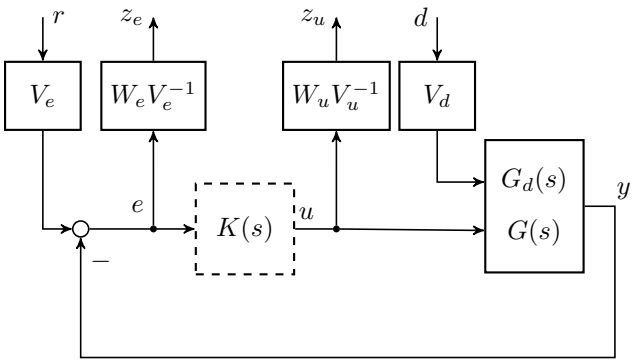

Fig. 1. Generic H_∞ weighting structure.

varying systems [8] and linear time varying systems [9]. The structure of the controllers has the form

$$\left[\begin{array}{c|c} \dot{\xi} \\ \hline u \end{array}\right] = \left[\begin{array}{c|c} A+BF+LC & L \\ \hline F & 0 \end{array}\right] \left[\begin{array}{c} \xi \\ \hline e \end{array}\right]. \tag{2}$$

The synthesis approach is based on sequentially solving a normalized coprime factorization and a state feedback problem as formalized in the following theorem.

Theorem 1 (observer-based controller synthesis): Let G be an linear time invariant (LTI) system. There exists an observer-based controller K as in (2) such that $||\mathcal{F}(G,K)|| \leq \gamma$ if there exist symmetric matrices $Z \in \mathbb{R}^{n_x \times n_x}$ and $Y \in \mathbb{R}^{n_x \times n_x}$ such that

$$Z > 0 \tag{3a}$$

$$\left[\begin{array}{cc} ZA + A^TZ - C^TC & ZB_d \\ B_d^TZ & -I \end{array}\right] < 0 \tag{3b}$$

and

$$\gamma > 1 \tag{4a}$$

$$Y > 0 \tag{4b}$$

$$\left[\begin{array}{ccc} YA^T + AY - \gamma B_u B_u^T & -YC^T & -Z^{-1}C^T \\ -CY & -\gamma I & I \\ -CZ^{-1} & I & -\gamma I \end{array}\right] < 0. \tag{4c}$$

Proof: Equations (3) are the existence conditions for the normalized left coprime factorization $M^{-1}N_d = G_d$ [7]. They yield the observer gain $L = -Z^{-1}C^T$ and establish

$$\hat{e} = Mr - N_d d. \tag{5}$$

Equations (4) are the state feedback existence conditions of Theorem 3 in [8] for the generalized plant formulated as

$$\left[\begin{array}{c} \dot{\xi} \\ \hline e \\ u \\ \xi \end{array}\right] = \left[\begin{array}{c|cc} A & L & B \\ \hline -C & I & 0 \\ 0 & 0 & I \\ I & 0 & 0 \end{array}\right] \left[\begin{array}{c} \xi \\ \hline \hat{e} \\ u \end{array}\right]. \tag{6}$$

They yield $F = -\gamma B_u^T Y^{-1}$ and establish

$$\left[\begin{array}{c} e \\ u \end{array}\right] = \left[\begin{array}{c} (I+GK)^{-1} \\ K(I+GK)^{-1} \end{array}\right] M^{-1}\hat{e}. \tag{7}$$

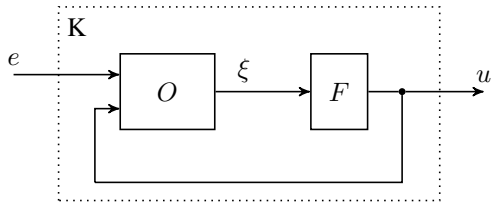

Fig. 2. Observer-based controller.

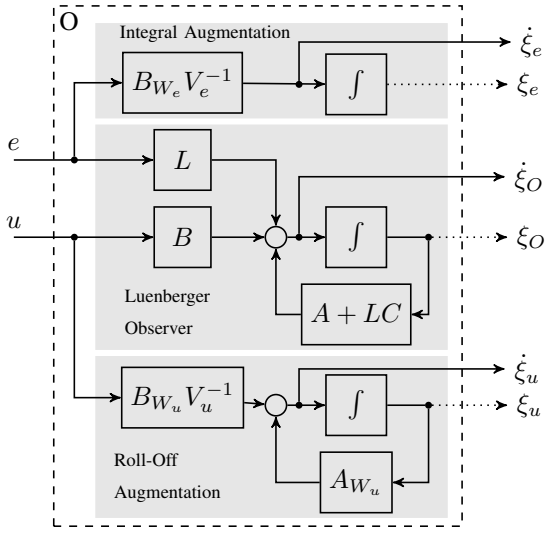

Fig. 3. Weight-augmented observer with state derivative output.

It was previously shown in [8] that the combination of (5) and (7) recovers the original mixed sensitivity problem (1). The property $|||[M \quad N_d]||| = 1$ of the normalized coprime factorization implies $|||[-N_d \quad M]||| = 1$ and it follows from submultiplicativity of the induced $\mathcal{L}_2$-norm that

$$\begin{aligned} \left|\left|\left|\left[\begin{array}{cc} -SG_d & S \\ -KSG_d & KS \end{array}\right]\right|\right|\right| &= \left|\left|\left|\left[\begin{array}{c} S \\ KS \end{array}\right] M^{-1} \left[-N_d \;\; M\right]\right|\right|\right| \\ &= \left|\left|\left|\left[\begin{array}{c} S \\ KS \end{array}\right] M^{-1}\right|\right|\right| \, |||[-N_d \;\; M]||| \\ &= \left|\left|\left|\left[\begin{array}{c} S \\ KS \end{array}\right] M^{-1}\right|\right|\right|. \end{aligned} \tag{8}$$

■

Theorem 1 can be used to solve a controller K as in (2) that minimizes the weighted mixed sensitivity problem depicted in Fig. 1. A step by step guide on the solution of the weighted problem is detailed in [8]. The key point is that the resulting controller has now a specific structure as shown in Fig. 2, where all the dynamics are in the observer O. Additionally, the observer itself is also highly structured as shown in Fig. 3. The observer consists of an integral augmentation through the weighting W_e, a roll-off augmentation through W_u and a classical Luenberger observer. This structure is specifically advantageous for adding anti-windup schemes as the integrators appear explicitly in the structure.

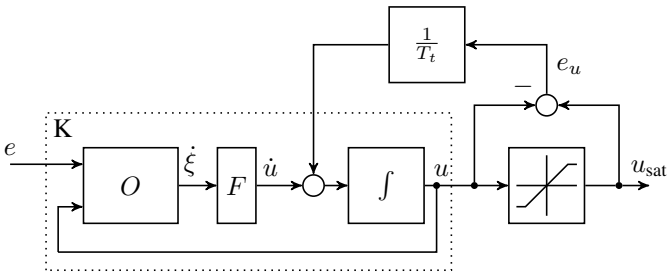

Fig. 4. Back-calculation anti-windup scheme for usage with an observer-based controller.

C. Anti-windup strategy

In a first step, the obtained observer-based controller is slightly modified in order to isolate the integrator. To achieve this, instead of the observer states ξ, the state derivatives $\dot{\xi}$ can be taken out of the structured observer, as seen in Fig. 3. Then, the multiplication with the observer gain

$$\dot{u} = F\dot{\xi} \tag{9}$$

is done as in the initial observer structure in Fig. 2. The integrator is then placed behind the feedback gain F in Fig. 4. Now that the integrator has been separated from the multi-input-multi-output (MIMO) controller's feedback gains, the implementation of an anti-windup method is a straight-forward task.

As the integrator states in Fig. 4 have now the physical meaning of the controller output, e.g. the anti-windup methods clamping or back-calculation can be used [10]. Clamping simply limits the integrator output to certain minimum or maximum values and stops the integration as long as the integrator output is in limit.

The back-calculation method [10] is convenient to use for preventing windup of the integrator in case of a variable or externally defined limit.

Fig. 4 shows the principle of the back-calculation method, where the difference of the unlimited and limited actuation commands, $e_u = u - u_{\text{sat}}$ is inserted into the integrator input. This gives the equation for the integrator input i:

$$i = \dot{u}\frac{1}{T_i} + e_u\frac{1}{T_t}, \tag{10}$$

where T_i is the integrator time constant, T_t is the time constant of the back-calculation block. In steady state, also during saturation, the feedback of e_u keeps the integrator input at zero, thus (10) can be reformulated to

$$e_u = -\dot{u}\frac{T_t}{T_i}. \tag{11}$$

Together with $e_u = u_{\text{sat}} - u$ this gives

$$u = u_{\text{sat}} + \dot{u}\frac{T_t}{T_i}. \tag{12}$$

Thus, during saturation the integrator output equals the limit value plus the derivative of the control variable u which is calculated via the observer and the static gain F.

Fig. 5. DLR's exemplary HALE aircraft representation. ©German Aerospace Center (DLR)

III. Observer-Based Path-Tracker Design with Anti-Windup for a HALE Aircraft

In this section the methodology for the observer based mixed sensitivity control design presented in section II is applied to a linear model of DLR's HALE aircraft [3] and verified in a non-linear simulator. Fig. 5 illustrates an example design of the described HALE aircraft [3].

A. Aircraft model

The mathematical model of the HALE aircraft includes non-linear rigid body aircraft equations of motion

$$\begin{bmatrix} M_b(\dot{V}_b + \Omega_b \times V_b) \\ I_b(\dot{\Omega}_b + \Omega_b \times (I_b\Omega_b)) \end{bmatrix} = \Phi_{ba} P_a^{\text{ext}}, \tag{13}$$

with the aircraft's mass M_b, its moment of inertia I_b, and the linear and rotational velocities V_b, Ω_b. External forces and moments P_a^{ext} on the right hand side are calculated as described in [11]. The model is augmented with a second order linear structural model

$$M_{ff}\ddot{u}_f + D_{ff}\dot{u}_f + K_{ff}u_f = \Phi_{fa}P_a^{\text{ext}}, \tag{14}$$

provided by [12] and [13]. In principle the structural dynamics in (14) are a second order differential equation with masses M_{ff}, stiffness matrix K_{ff}, damping matrix D_{ff} and the modal displacement u_f. Finally, the aerodynamics are modeled via the vortex lattice method (VLM). A detailed description on these aerodynamics can be found in [11]. Deriving a linear model of the aircraft in the standard form

$$\begin{bmatrix} \dot{x} \\ y \end{bmatrix} = \left[\begin{array}{c|cc} A & B_u & B_d \\ \hline C & D_u & D_d \end{array}\right] \begin{bmatrix} x \\ u \\ d \end{bmatrix} \tag{15}$$

with the state vector x, its derivative $\dot{x}$, the input vector u, the output vector y, the scalar disturbance d and the state space matrices A, B_u, B_d, C, D_u, and D_d, finally enables the application of a linear control design method. Therefore, the non-linear aircraft equations are linearized at a steady state operating point with airspeed defined by $V_{\text{TAS}} = V_{\text{max}}$ and altitude h = 20 km. A low order approximation of the aircraft's longitudinal dynamics is obtained via truncation of

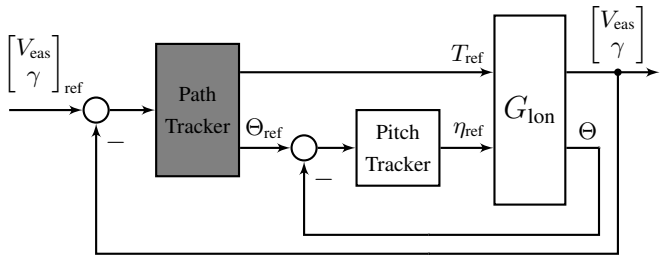

Fig. 6. Controller structure illustration.

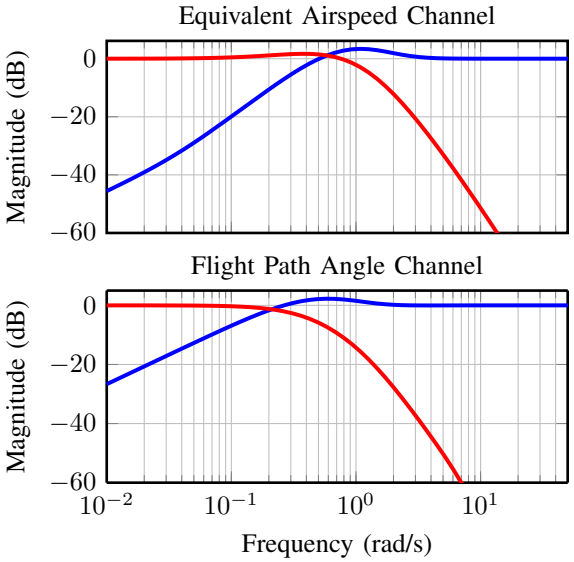

Fig. 7. Output sensitivity S (——) and complimentary sensitivity T (——) for the mixed-sensitivity path-tracker.

the lateral modes as well as flexible modes far beyond the actuator bandwidth.

For the derived aircraft model for the controller design, the state vector x includes the angle of attack α, pitch rate q, pitch attitude θ, airspeed V, the involved structural modes U_f and their derivatives dU_f. The input vector u includes the elevator deflection η and thrust setting T and the output vector y includes pitch angle θ, flight path angle γ, and the true airspeed V_{TAS}. Finally, the disturbance d is a wind disturbance on the aircraft.

B. Controller design

For the MIMO controller synthesis, the linear model of the operation point at maximum speed and maximum altitude is chosen since this point shows the highest frequency and lowest damping values of the pitch motion throughout the flight envelope. It is assumed, that deriving a controller ensuring adequate closed loop stability and performance for this "worst-case" point, the controller enables even better results for the lower flight speeds and lower altitudes. The block diagram in Fig. 6 illustrates the interconnection of the path-tracker with an inner-loop feedback controller and the the longitudinal aircraft dynamics G_{lon}. First, the pitch-tracker of the standard proportional-integral form

$$\eta_{\text{ref}} = k_p e_\Theta + k_i \int e_\Theta \text{dt} \tag{16}$$

with the two controller gains k_p and k_i is designed as an inner loop controller. For this inner loop the reference variable is the pitch attitude Θ_{ref} in order to derive the control error $e_\Theta = \Theta_{\text{ref}} - \Theta$ via the feedback of the pitch angle Θ. The pitch tracker is designed with a bandwidth of 2 rad/s in order to ensure a fast and well damped inner system. More details on the actual inner loop controller design and its specifications are provided in [2].

For the path-tracker controller synthesis, the weighting scheme depicted in Fig. 1 is used. The required scaling of the inner loop dynamics for the H_∞ controller design is considered via $V_e = [1, 5\pi/180]I_2$ on the inner loop outputs, i.e., assuming a maximum velocity deviation of 1 m/s from the trim point and a maximum Flight Path Angle (FPA) deviation of 5 degrees. $V_d = 1$ m/s is equally applied for the disturbance input. For the input scaling of the inner loop system $V_u = [0.2, 5\pi/180]I_2$ is applied, i.e., a maximum authority of 0.2 as achievable thrust to weight ratio and a maximum of 5 degrees in pitch attitude reference.

For the performance weight W_e a bandwidth of 0.25 rad/s is targeted in both the velocity and the FPA channel. These 0.25 rad/s are well below the the pitch tracker's inner loop bandwidth of of 2 rad/s as well as the available designed bandwidth of the thrust channel, which is assumed to be above 1 rad/s. To support this, the roll-off filter W_u is selected with a bandwidth of 0.5 rad/s in both input channels. The resulting closed loop sensitivity and complementary sensitivity functions for the velocity and for the FPA channel are depicted in Fig. 7. Considering a bandwidth definition at the intersection of the sensitivity function with the -3 dB line [4], leads to a bandwidth of about 0.4 rad/s in the velocity channel and 0.2 rad/s in the FPA channel. For the anti-windup augmentation, the parameter T_t in (10)-(12) is selected equal to the integrator time constant $T_i = 1$.

C. Non-linear simulation

The verification of the designed control system is performed using a non-linear model of the aircraft dynamics as presented in (13) and (14) augmented with the controller designed herein. The results of the non-linear closed loop simulations are presented in Fig. 8. The simulated scenario is a climb maneuver between $t = 10$ s until $t = 35$ s with a step-wise commanded flight path angle of 5 deg during this time. The results in Fig. 8 compare the described maneuver for the developed control system with an engine saturation limit beyond the actual requirement (blue), with an artificial saturation limit of the engine at approximately 150 N per engine with (green) and without (red) anti-windup functionality in the control system. Note, that this artificial limit is chosen to allow for a better comparison of the result. The actual saturation limit of the engine is higher than the presented one.

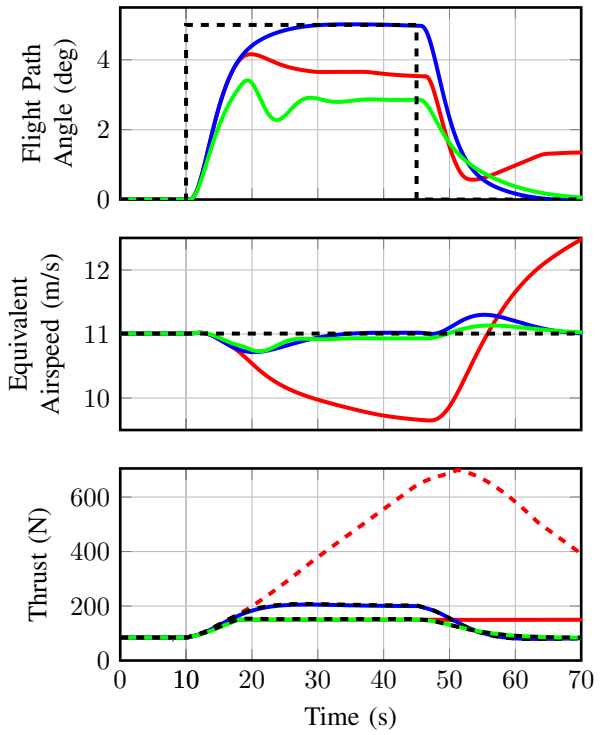

Fig. 8. Non-linear closed loop simulation of the observer-based path-tracker in nominal operation (——) and with thrust control variable in saturation without anti-windup (——) and with anti-windup active (——).

The nominal case (blue) shows adequate performance with a settling time of less than 20 s and no overshoot of the flight path angle response in the first diagram. This corresponds to the design goal defined in the mixed-sensitivity controller design. Furthermore, the cross-coupling between flight path command and airspeed, visible via the second diagram, is limited to 0.3 m/s. Considering linearity, this corresponds to about 0.06 m/s per degree of flight path angle command. The achieved (blue) and required thrust (black) are depicted in the third diagram. In the scenario without saturation the lines are nearly exactly above each other, as only the linear engine dynamics lie between the two signals.

As mentioned above, in a second scenario the thrust is limited to a maximum value of 150 N. The saturation is clearly visible in the third diagram, as for both, the scenario with and without anti windup the actual thrust signals do not increase over 150 N (green and solid red lines). In the scenario without anti-windup, however, severe integrator windup is encountered in the thrust command (red dashed line in third diagram). This windup effect results in large airspeed (red line in second diagram) deviations and no adequate tracking even after the flight path command is taken back to zero at 35 s in the simulation. To avoid this undesired behavior, anti-windup augmentation in the form of back-calculation is introduced and added to the observer-based controller. The green lines in Fig. 8 depict this scenario which shows similar small deviation of the airspeed from the command value during the flight path angle command input as seen in the nominal case (green vs. blue lines in the middle plot in Fig. 8). Moreover, as soon as the flight path reference returns to zero, the nominal controller performance is restored instantaneously. The FPA is tracked with a higher control error during the FPA command when anti-windup is active. This is due to the smaller velocity error. In case no anti-windup is used the increased velocity error induces a higher pitch angle reference θ_{ref} due to the cross-coupling in the controller.

IV. Comparison to Total Energy Control

A longitudinal autopilot concept which offers decoupling of airspeed and flight path angle is the Total Energy Control System TECS. A control strategy initially introduced in the early 80's by A. Lambregts [14] and subsequently flight tested by NASA and Boeing [15]. It has been applied in previous HALE design projects as well as proven in flight tests [16].

The TECS control law is based on the principle of the overall energy of the aircraft, i.e. $E = E_{\text{pot}} + E_{\text{kin}}$. With the small angle approximation $\dot{h} \simeq V\gamma$ the derivative of the total energy equation is given by

$$\dot{E} = mg\dot{h} + mV\dot{V} \simeq mgV\left(\gamma + \frac{\dot{V}}{g}\right). \tag{17}$$

Assuming that the increase in drag ΔD is small compared to the thrust increase ΔT in (18), an energy change $\dot{E}$ can directly be related to a thrust command T_{cmd}. Introducing the specific total energy rate $\dot{E}_S = \dot{E}/(mgV)$ and considering the control errors in flight path angle and equivalent airspeed results in

$$\begin{aligned} \Delta\dot{E}_S &= (\gamma_{\text{cmd}} - \gamma) + (\dot{V}_{\text{cmd}} - \dot{V})/g \\ &= (\Delta T_{\text{cmd}} - \Delta D)/(mg) \simeq T_{\text{cmd}}/(mg), \end{aligned} \tag{18}$$

describing the commanded specific energy rate change. Finally, a proportional-integral (PI) control law for the thrust can be defined by

$$\frac{T_{\text{cmd}}}{mg} = K_{TI}\int \Delta\dot{E}_S dt - K_{TP}.\dot{E}_S \tag{19}$$

To derive the second command signal $\delta\Theta_{\text{cmd}}$, the specific energy distribution $\dot{D}_s$ between kinematic and potential energy rate is simply defined by the difference of the two energy types,

$$\dot{D}_S = -E_{\text{S,pot}} + E_{\text{S,kin}} = -\gamma + \frac{\dot{V}}{g}. \tag{20}$$

The specific energy distribution can be fed back due to the substitution in (20) by the measurements γ and $\dot{V}$. To enable a feedback loop substituted measurements are subtracted their demands

$$\Delta\dot{D}_S = \dot{D}_{S,\text{cmd}} - \dot{D}_S = -(\gamma_{\text{cmd}} - \gamma) + \frac{(\dot{V}_{\text{cmd}} - \dot{V})}{g}. \tag{21}$$

Finally, using the assumption that commanded energy distribution rate is proportional to the commanded pitch attitude, i.e., $\Delta\dot{D}_S \propto \Delta\Theta_{\text{cmd}}$, the outer loop control law

$$\delta\Theta_{\text{cmd}} \propto K_{DI}\int \Delta\dot{D}_S dt - K_{DP}\dot{D}_S \tag{22}$$

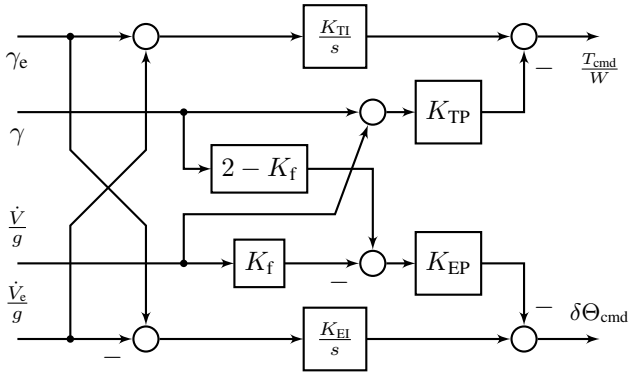

Fig. 9. TECS controller architecture.

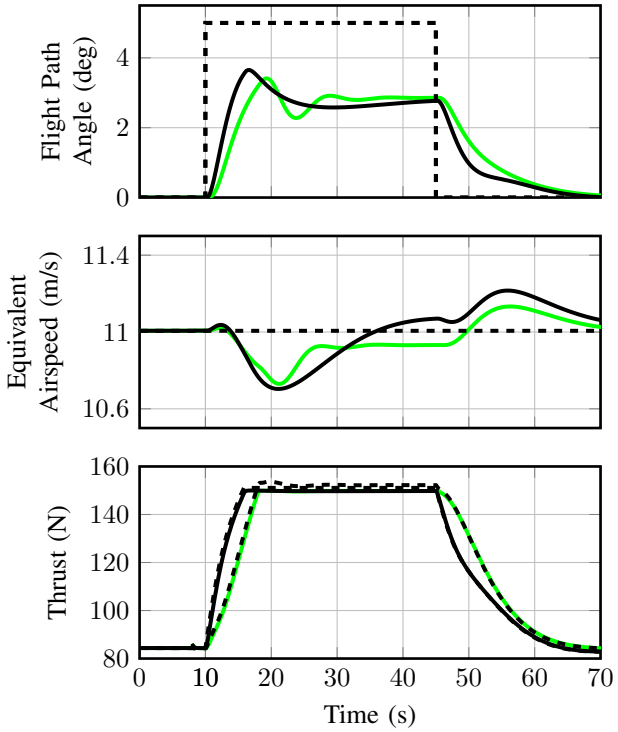

Fig. 10. Non-linear closed loop simulation of the observer-based path-tracker with Anti-Windup compensation (——) in comparison to TECS (——) for thrust in limits.

can be derived. The used TECS structure is depicted in Fig. 9. The proportional and integral gains for the specific energy rate in (19) and specific energy distribution (22) are tuned in order to achieve a bandwidth of 25% the inner loop bandwidth, together with satisfactory gain and phase margins as well as disturbance rejection specifications.

Fig. 10 depicts the results for the same scenario as in Fig. 8. In this scenario, the results using the TECS path-tracker described above are compared to the observer-based mixed sensitivity path-tracker designed within this work. It can be seen that both approaches achieve similar performances and satisfy the tracking requirements. A satisfactory suppression of cross-coupling between flight path angle and airspeed is achieved.

V. Conclusions

In this paper the design and verification of a path-tracker for the application on a HALE aircraft is presented. The H_∞-based control design deviates from a classical H_∞ design approach so that the state feedback observer and the state feedback controller are provided explicitly. This poses the advantage in the controller implementation that its integrator can be isolated and anti-windup augmentation can be considered easily. The application to the HALE aircraft and the gathered results of the non-linear simulation highlight the importance of integrator windup protection for the H_∞ based control system. The results prove that the observer-based mixed sensitivity approach is capable of achieving similar results as the well-known TECS architecture. However, due to the application of standard MIMO control design methods, the tuning becomes systematic and drives the design away from pure heuristics.

References

[1] J. Theis, N. Sedlmair, F. Thielecke, and H. Pfifer, "Observer-based LPV control with anti-windup compensation: A flight control example," *IFAC-PapersOnLine*, vol. 53, no. 2, pp. 7325–7330, 2020.

[2] C. Weiser and D. Ossmann, "Baseline flight control system for high altitude long endurance aircraft," in *AIAA SciTech 2022 Forum*. American Institute of Aeronautics and Astronautics, 2022.

[3] German Aerospace Center (DLR), "DLR develops an unmanned stratospheric aircraft," 2021. [Online]. Available: https://www.dlr.de/content/en/articles/news/2021/02/20210421_dlr-develops-an-unmanned-stratospheric-aircraft.html

[4] S. Skogestad and I. Postlethwaite, *Multivariable Feedback Control*. John Wiley & Sons, 2005.

[5] J. Theis, H. Pfifer, and P. Seiler, "Robust modal damping control for active flutter suppression," *Journal of Guidance, Control, and Dynamics*, vol. 43, no. 6, pp. 1056–1068, 2020.

[6] K. Glover and D. McFarlane, "Robust stabilization of normalized coprime factor plant descriptions with H_∞-bounded uncertainty," *IEEE Transactions on Automatic Control*, vol. 34, no. 8, pp. 821–830, 1989.

[7] D. McFarlane and K. Glover, Eds., *Robust Controller Design Using Normalized Coprime Factor Plant Descriptions*. Springer-Verlag Berlin Heidelberg, 1990.

[8] J. Theis and H. Pfifer, "Observer-based synthesis of linear parameter-varying mixed sensitivity controllers," *International Journal of Robust and Nonlinear Control*, vol. 30, no. 13, pp. 5021–5039, 2020.

[9] F. Biertümpfel, J. Theis, and H. Pfifer, "Observer-based synthesis of finite horizon linear time-varying controllers," in *American Control Conference (ACC)*, 2022, accepted.

[10] K. Åaström and T. Hägglund, *PID controllers*. International Society for Measurement and Control, 1995.

[11] T. Kier, G. Looye, and J. Hofstee, "Development of aircraft flight loads analysis models with uncertainties for pre-design studies," in *International Forum on Aroelasticity and Structural Dynamics (IFASD)*, 2005.

[12] T. Kier and J. W. Hofstee, "Varloads - eine Simulationsumgebung zur Lastenberechnung eines voll flexiblen, freifliegenden Flugzeugs," in *Deutscher Luft- und Raumfahrtkongress (DLRK)*, 2004.

[13] A. Voß, V. Handojo, C. Weiser, and S. Niemann, "Preparation of loads and aeroelastic analyses of a high altitude, long endurance, solar electric aircraft," in *Aerospace Europe Conference*, 2020.

[14] A. A. Lambregts, "TECS generalized airplane control system design – an update," in *Advances in Aerospace Guidance, Navigation and Control*. Springer Berlin Heidelberg, 2013, pp. 503–534.

[15] K. R. Bruce, J. R. Kelly, and L. J. Person, "NASA B737 flight test results of the Total Energy Control System," in *AIAA Astrodynamics Conference*, 1986.

[16] N. Kastner and G. Looye, "Generic TECS based autopilot for an electric high altitude solar powered aircraft," in *Proceedings of the EuroGNC 2013, 2nd CEAS Specialist Conference onGuidance, Navigation & Control*, 2013, pp. 1324–1343.